

Design, synthesis, and biological evaluation of novel azaspirooxindolinone derivatives as potent inhibitors of ITK and BTK-positive cancers

Gopal Muddasani,^{1, 2} Naveen Kumar Rampeesa,^{1, 2} Sreenivasareddy Anugu,¹ Pullareddy Muddasani,³ Soňa Gurská,^{4, 5} Petr Džubák,^{4, 5} Marián Hajdúch,^{4, 5} Viswanath Das,^{4, 5, *} Rambabu Gundla^{2, *}

¹ Aragen Lifesciences Pvt. Ltd, Medicinal Chemistry Laboratory Division, Survey No: 125(Part) & 126, IDA Mallapur, Hyderabad 500076, India

² Department of Chemistry, School of Science, GITAM University, Hyderabad 502102, Telangana, India

³ NATCO Research Center, Sanath Nagar Industrial Area, Sanath Nagar, Hyderabad, Telangana, 500018.

⁴ Institute of Molecular and Translational Medicine, Faculty of Medicine and Dentistry Palacký University and University Hospital Olomouc, Hněvotínská 1333/5, 77900 Olomouc, Czech Republic

⁵ Czech Advanced Technologies and Research Institute (CATRIN), Institute of Molecular and Translational Medicine, Palacký University Olomouc, Křížkovského 511/8, 77900, Olomouc, Czech Republic

*Correspondence to: Viswanath Das (Email: viswanath.das@upol.cz, Tel.: +420 585 632 111; ORCID ID: 0000-0001-5973-5990) and Rambabu Gundla (Email: rgundla@gitam.edu, Tel.: +91-9849869933)

Highlights

- Synthesized azaspirooxindolinone derivatives exhibit potent cytotoxicity in both ITK/BTK-negative and -positive cancer cell lines.
- Compounds **3d** and **3j** demonstrate high cytotoxicity, indicating potential dual inhibition against ITK and BTK.
- Compounds **3a** and **3e** display specificity in targeting ITK-positive cancer cells, while compounds **3f** and **3g** target BTK-positive cells.

- Active compounds show no cytotoxic effects on non-cancer cell lines, suggesting potential selectivity for cancer cells.
- These findings highlight the promising cytotoxic activity of azaspirooxindolinone derivatives, warranting further investigation into their therapeutic potential.

Abstract

Bruton's tyrosine kinase (BTK) and Interleukin-2-inducible T-cell kinase (ITK) are two important members of the Tec family with crucial roles in immune system function. Deregulation in ITK and BTK activity is linked to several hematological malignancies, making them key targets for cancer immunotherapy. In this study, we synthesized new azaspirooxindolinone derivatives and evaluated their cytotoxic activity against ITK/BTK-negative and -positive cancer cell lines. Compounds **3d** and **3j** exhibited high cytotoxicity in both ITK-positive Jurkat ($IC_{50} = 3.58 \mu\text{M}$ and $4.16 \mu\text{M}$, respectively) and BTK-positive Ramos ($IC_{50} = 3.06 \mu\text{M}$ and $1.38 \mu\text{M}$, respectively) cell lines, indicating their potential dual activity against ITK and BTK. **3a** and **3e** showed high cytotoxicity specifically in ITK-positive Jurkat cells with IC_{50} values of $9.36 \mu\text{M}$ and $10.85 \mu\text{M}$, respectively. Compounds **3f** and **3g** were highly cytotoxic specifically in Ramos cells with IC_{50} values of $1.82 \mu\text{M}$ and $1.42 \mu\text{M}$, respectively. None of the active compounds exhibited cytotoxic effects against non-cancer cell lines ($IC_{50} > 50 \mu\text{M}$). These findings suggest that the synthesized azaspirooxindolinone derivatives, particularly compounds **3d** and **3j**, hold promise as dual inhibitors for ITK and BTK-positive cancers, while compounds **3a**, **3e**, **3f**, and **3g** demonstrate potential as specific inhibitors, warranting further investigation.

Keywords

Anti-cancer derivatives; Azaspirooxindolinones; Bruton's tyrosine kinase; Interleukin-2-inducible T-cell kinase; Molecular docking

Introduction

Interleukin-2-inducible T-cell kinase (ITK) and Bruton's tyrosine kinase (BTK) play pivotal roles in the immune system and have been implicated in human diseases¹. ITK, primarily expressed in T-cells, regulates T-cell activation and differentiation. Dysregulation of ITK has been associated with various cancers², highlighting its

potential as a therapeutic target in cancer immunotherapy. On the other hand, BTK, predominantly expressed in B cells, is a key component of B-cell receptor signaling. Aberrant BTK activity has been linked to B-cell malignancies, such as B-cell lymphomas and leukemia³. Targeting BTK, as demonstrated by drugs like Ibrutinib, has shown clinical success in treating certain hematologic malignancies⁴. The roles of ITK and BTK in immune cell signaling underscore their significance in cancer and other human pathogenesis^{5,6}, presenting opportunities for developing targeted therapies against these kinases in the context of human diseases.

Current research in developing inhibitors targeting ITK and BTK holds promise for advancing therapeutic options, especially for immune-related disorders and cancers⁷. ITK inhibitors are being explored for their potential in modulating T-cell responses and immune-related diseases, focusing on improving specificity and efficacy^{8,9}. Meanwhile, BTK inhibitors continue to be a subject of intense investigation, especially in hematological malignancies¹⁰. Amino thiazoles by Bristol-Myers Squibb, amino benzimidazoles by Boehringer Ingelheim, indoles by Sanofi-Aventis, and pyridones by Vertex were among the early compounds designed to selectively target ITK¹¹. Ibrutinib, a BTK inhibitor, has already demonstrated clinical success in conditions like chronic lymphocytic leukemia and mantle cell lymphoma¹². Ibrutinib was initially designed as a BTK inhibitor but was later found to inhibit ITK due to structural homology¹³. Ongoing research aims to enhance the selectivity and minimize the off-target effects of these inhibitors, paving the way for more effective and safer treatments for immune-related and oncological conditions.

In the structure-activity relationship (SAR) studies of our previous series of compounds¹⁴, among the six structurally similar compounds (active – **II**, **III**, **IV**; and inactive – **V**) (**Fig. 1**), the critical structural variation leading to the loss of anti-proliferative activity in compound **V** was due to the replacement of the benzodioxyl group with a 3,4,5-trimethoxyphenyl group at the C-5 position of azaspirooxindoles. This indicated that the presence of the benzodioxyl group in compound **V** is vital for its cytotoxic activity in ITK and BTK-high cell lines. Another common structural feature present in the active compounds, demonstrating excellent anti-cancer activity, is the α , α -dimethyl functionality (geminal/cyclopropyl) with a heteroatom (fluorine) attached to the carbonyl carbon of the carboxamide functional group (**Fig. 1**). These results

encouraged us to design a new series of compounds based on SAR studies by varying the hydrophilic groups/atoms on α -carbon of the carbonyl group of azaspirooxindoles, keeping with the C-5 benzodioxyl group. With these modifications, we designed and synthesized twelve new compounds along with two new compounds with C-5 aryl modifications and one trifluoromethyl sulphonamide derivative. In this study, we report the synthesis of new azaspirooxindolinone derivatives and their biological activity in a panel of cancer cell lines comprising ITK and BTK-high cancer cell lines.

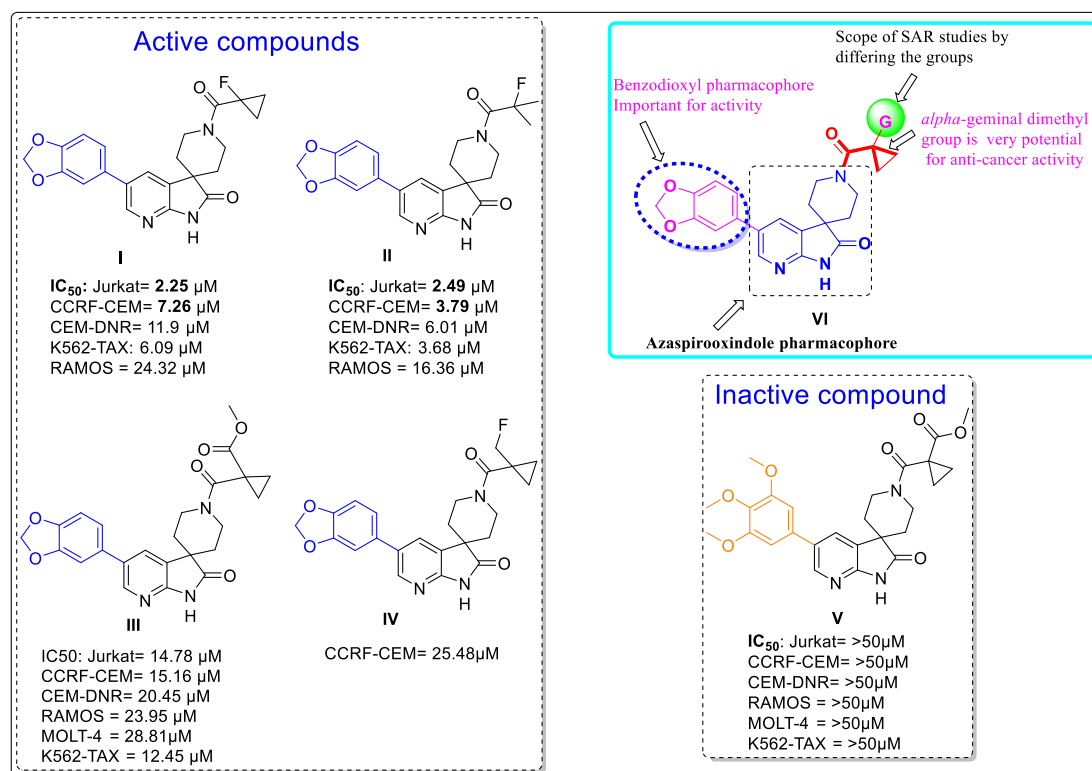


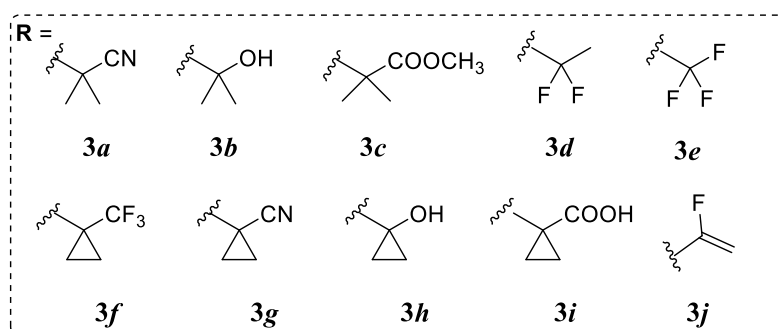
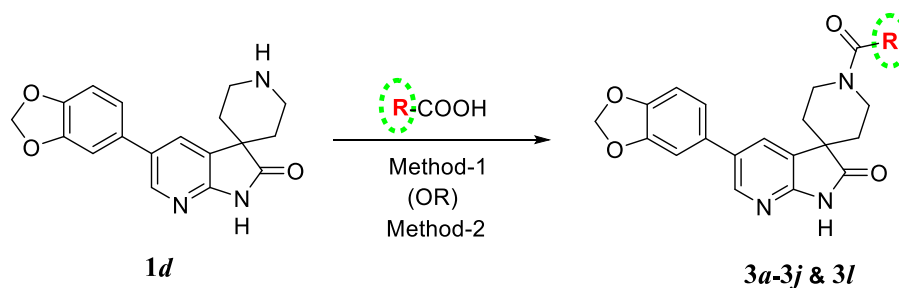
Figure 1. Design and SAR studies towards new series compounds.

Results and Discussions

Chemistry

The synthesis of target compounds is outlined in **Schemes 1** and **2**. Reacting compound 5'-(benzo[d][1,3]dioxol-5-yl) spiro[piperidine-4,3'-pyrrolo[2,3-b]pyridin]-2'(1'H)-one (**1d**)¹⁵ with corresponding carboxylic acids using the HATU coupling agent and DIPEA in N, N-dimethyl formamide afforded compounds **3a** to **3j** and **3l** in good yields.

The ^1H NMR chemical shift values of geminal dimethyl protons of **3a** are observed at δ 1.58 ppm. In the ^{13}C NMR, cyano carbon appeared at δ 201.3 ppm. In ^1H -NMR of compound **3b**, the *gem*-dimethyl proton signals were observed at δ 1.50 and 1.62 ppm. In ^{13}C NMR, the three carbonyl signals were shifted to a downfield at δ 162.61 and 180.19 ppm. The ethyl signals of ester of compound **3c** were spotted as a triplet at δ 1.23 ($J = 6.8$ Hz) and quartet at δ 4.15 ($J = 6.8$ Hz) ppm. In ^1H -NMR of compound **3d**, the triplet at δ 1.89 with a high " J " value of 20.0 Hz is evidence of methylene protons attached to geminal di-fluorine atoms. In ^{13}C NMR of **3d**, the carbon and fluorine two bond coupling appeared as a doublet at δ 21.92 and 161.28 ppm with coupling constant values of $J_{\text{C}(2)\text{-F}} = 24.8, 28.8$ Hz for carbonyl carbon and methyl carbon, respectively. In the ^{13}C NMR of **3e**, two bonds of a carbon-fluorine atom of carbonyl carbon appeared as doublet $J_{\text{C}(2)\text{-F}}$ ($J = 50.8$ Hz) at δ 155.0 ppm. The cyclopropyl ring protons of compound **3f** appeared as two sets of multiplet between δ 1.21-1.38 ppm. ^1H -NMR signals of compound **3h** for cyclopropyl ring proton were seen at δ 0.78-0.99 ppm. The cyclopropyl ring protons of compound **3i** appeared as a multiplet at δ 1.21-1.41 ppm, and two D_2O exchangeable singlets for carboxylic acid and amide protons were spotted at δ 12.58 and 11.13 ppm, respectively.

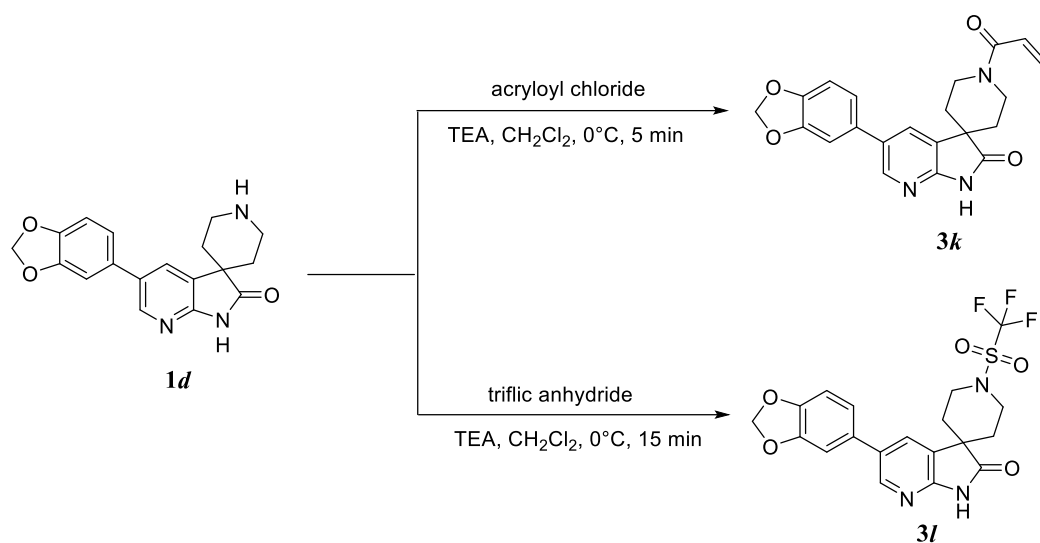


Method-1: HATU, DIPEA, DMF, rt, 2 h; **Method-2:** T₃P, DIPEA, DMF, rt, 16 h

Scheme 1. Synthetic scheme of N-acyl derivatives of azaspirooxindoles.

For the preparation of compound **3j**, the acid-amine coupling between 2-fluoroacrylic acid and corresponding amine (**1d**) was performed under standard conditions using T₃P (50% solution in ethyl acetate) as coupling reagent and triethylamine base in DMF solvent at ambient temperature for overnight. For compound **3j**, the signals of alkene protons appeared as two doublets of doublets at δ 5.16-5.33 ppm.

Amidation of **1d** with acryloyl chloride gave the corresponding derivative **3k**. ¹H-NMR spectra showed three doublets of doublet signals at δ 6.82, 6.15, and 5.71 ppm with a high coupling constant (*J*) of 16.8 Hz for *trans* protons of olefin. The reaction of compound **1d** with triflic anhydride presence of triethylamine in dichloromethane resulted in 5'-(benzo[d][1,3]dioxol-5-yl)-1-((trifluoromethyl)sulfonyl)spiro[piperidine-4,3'-pyrrolo[2,3-b]pyridin]-2'(1'H)-one **3l**. The formation of compound **3l** was confirmed by ¹H-NMR, which showed the downfield shift in piperidine ring protons. Besides, the LC-MS spectrum indicated the molecular ion peaks at *m/z* 456.1 (M+H)⁺.



Scheme 2. Synthetic scheme of compound **3k** and **3l**.

Docking-based Virtual Screening

A docking study was conducted to get insight into the binding affinity and the intermolecular interactions of azaspirooxindolinone derivatives with the ITK enzyme. ITK complexed with an inhibitor, Ibrutinib (PDB ID- 5P9J), was used for docking

analysis. Ibrutinib was used as a standard drug to screen azaspirooxindolinone derivatives.

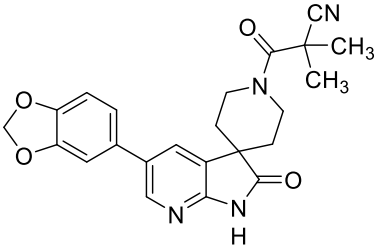
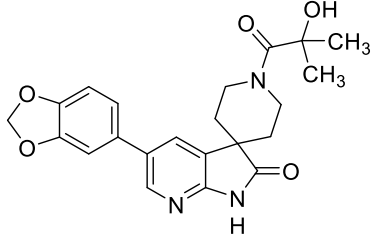
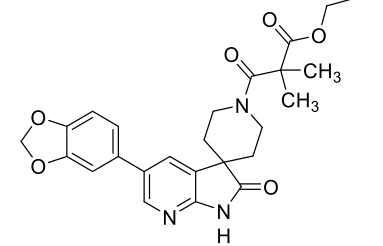
Ibrutinib is an irreversible BTK inhibitor that prevents downstream B-cell receptor activation¹⁶. It is interesting to note that ITK and BTK exhibit significant sequence and functional homology, and both have an ibrutinib inhibition motif composed of a tyrosine (Tyr) that is SH3 auto phosphorylatable and a cysteine (Cys) that is covalently bound in the hinge region that connects the C and N lobes of the active site¹⁷. Ibrutinib is thought to be the first therapeutically effective ITK inhibitor due to the striking similarity between BTK and ITK. Ibrutinib binds to ITK irreversibly and suppresses Th2 cell activation after TCR stimulation¹³.

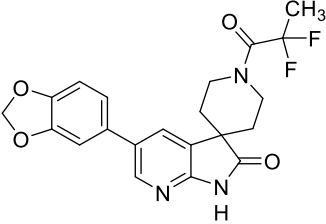
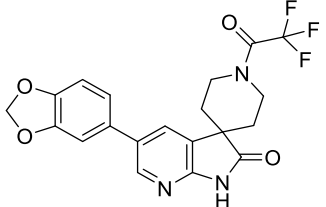
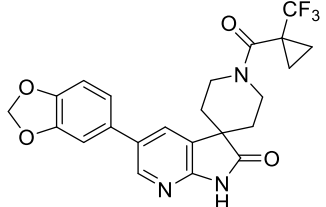
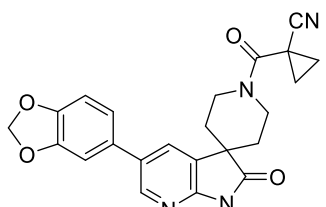
All 12 derivatives of azaspirooxindolinone were docked into the binding site of ITK in the current study. We compared the binding energies and molecular interactions of azaspirooxindolinone derivatives with those of Ibrutinib to select compounds (**Table 1**). The docking energy of Ibrutinib was -9.2 kcal/mol, whereas **3a**, **3e**, **3f**, **3g**, and **3i** exhibited higher docking energies to the active site residues of the ITK. Compound **3e** has the highest docking score of -9.7 kcal/mol. Although it lacks hydrogen bonds, it exhibits attractive charge interactions with Lys391, Pi Amide stacking with Phe374, and Alkyl bonding with Met503. Compounds **3a**, **3f**, **3g**, and **3i** exhibited the second-highest docking score (9.4 kcal/mol). Compound **3k** stands out with the lowest docking energy, recording -8.7 kcal/mol among all the compounds.

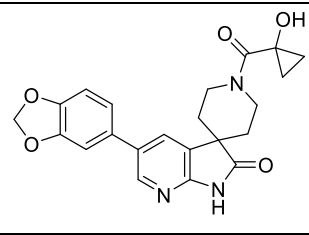
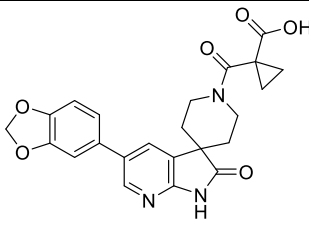
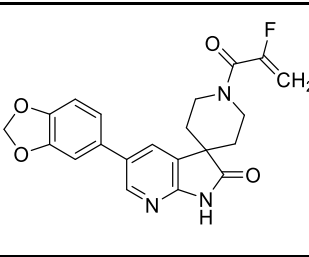
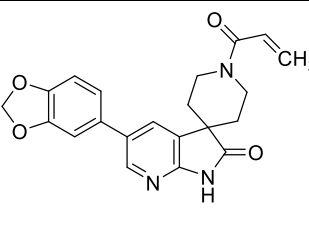
A pharmacophore-based virtual screening was done to identify possible ITK inhibitors in a three-dimensional model of ITK inhibitors¹⁹. Certain compounds were found to establish hydrogen bond interactions with Met438 and Lys391, indicating the formation of essential interactions between the compound and the ITK protein. The compounds displaying strong interactions were identified as potential effective ITK inhibitors. The synthesized derivatives also interacted with the investigated protein by binding to specific amino acids. Therefore, further research could explore their potential as inhibitors of ITK. Another study illustrated a comparable binding method between various pyrazolyl-indole derivatives and ITK²⁰. Interactions with the amino acids Glu436, Met438, and Phe435 were identified during docking. Further, Wang *et al.*, found that the side chains of Phe435, Lys391, Val377, and Ala389 produced a distinct hydrophobic pocket during interactions with the ITK¹⁹. It is possible to increase

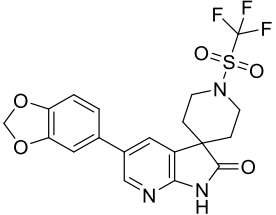
inhibitory efficacy against ITK by introducing substituents at the C6 position of the indazole moiety to occupy the hydrophobic pocket.

Table 1. Docking scores and amino acid interactions of synthesized compounds.

Compound name	Structure	Docking score	Amino-acid interactions
3a		-9.4	Val507, Asn487, Asp482, Thr504, Met503, Lys391, Phe374, Gln373, Ile369, Ser371-Van der Waals; Arg486, Tyr512-Conventional Hydrogen Bonds; Asp500, Gly372-Carbon Hydrogen Bond; Lue489, Ala389, Val377-Alkyl
3b		-9.0	Tyr512, Asn487, Asp482, Lys391, Phe435, Phe437, Gly441, Gly372, Gln373-Van der Waals; Arg486, Met438, Ser371-Conventional Hydrogen Bond; Asp486, Glu436-Carbon Hydrogen Bond; Asp500-Unfavourable Acceptor-Acceptor; Ala389, Leu489, Val377, Ile369-Pi Alkyl
3c		-9.0	Gly372, Leu489, Gly441, Met438, Gly370, Val377, Lys391, Ile393, Val507, Asn487-Van der Waal; Cys442-Conventional Hydrogen Bond; Gln373-Carbon Hydrogen Bond; Asp500-Attractive Charge; Phe374-Amide Pi Stacked; Met398-Pi Sulfur; Ala389, Ile369, Phe437-Alkyl; Met503, Arg486-Pi Alkyl

3d		-9.0	Gly372, Leu489, Gly441, Met438, Gly370, Val377, Lys391, Ile393, Val507, Asn487-Van der Waals; Asp500-Attractive Charge; Cys442-Conventional Hydrogen Bond; Gln373-Carbon Hydrogen Bond; Phe374-Amide Pi Stacked; Met398-Pi Sulfur; Ala389, Ile369, Phe437-Alkyl; Met503, Arg486-Pi Alkyl
3e		-9.7	Cys442, Val377, Ile369, Ala389, Met438, Gly441, Asp500, Leu489, Gly372, Gln373, Ile393-Van der Waal; Lys391-Attractive Charge; Phe374-Amide Pi Stacked; Met503-Alkyl
3f		-9.4	Thr504, Arg486, Phe374, Lys391, Phe437, Gly441, Ser371, Gly372, Asp500, Val507; Met503-Conventional Hydrogen Bond; Asn487, Tyr512-Conventional Hydrogen Bond; Met438-Carbon Hydrogen Bond; Asp482, Gln373-Halogen (Fluorine); Leu489, Ala389, Val377, Ile369-Alkyl
3g		-9.4	Thr504, Arg486, Phe374, Lys391, Phe437, Gly441, Ser371, Gly372, Asp500, Val507-Van der Waals; Met503-Conventional Hydrogen Bond; Asn487, Tyr512-Conventional Hydrogen Bond; Met438-Carbon Hydrogen Bond; Asp482, Gln373-Halogen (Fluorine); Leu489, Ala389, Val377, Ile369-Alkyl

3h		-9.0	Lys391, Leu489, Ile369, Ala389, Phe437, Glu436, Val419, Val377, Phe435, Cys442, Asn487, Arg486, Gln373, Tyr512, Asp482, Thr504, Phe374, Val507-Van der Waal; Met438-Conventional Hydrogen bond; Asp500-Attractive Charge
3i		-9.4	Ser371, Gly372, Tyr512, Gln373, Arg486, Asp482, His480, Thr504, Met503, Phe374, Lys391, Met438,Ile369-Van der Waal; Asn487, Asp500-Conventional Hydrogen Bond; Val377, Ala389, Leu489-Alkyl
3j		-9.1	Glu436, Val419, Val377, Phe435, Cys442, Asn487, Arg486, Gln373, Tyr512, Asp482, Thr504, Phe374, Val507-Van der Waal; Met438-Conventional Hydrogen Bond; Asp500-Attractive Charge
3k		-8.7	Cys442, Ile369, Leu489, Ala389, Phe437, Met438, Asp500, Val377, Gly372, Gln373, Ile393-Van der Waal; Lys391-Attractive Charge; Gly441-Carbon Hydrogen Bond; Phe374-Pi Amide Stacked; Met503-Alkyl

3/		-8.9	Ile393, Met438, Lys391, Leu489, Ala389, Ile369, Val377, Gly372, Asn487, Val507-Van der Waal; Gly441-Carbon Hydrogen Bond; Arg486-Conventional Hydrogen Bond; Asp500-Attractive Charge; Phe374-Amide Pi Stacked; Met398-Pi Sulfur; Met503-Alkyl
----	---	------	--

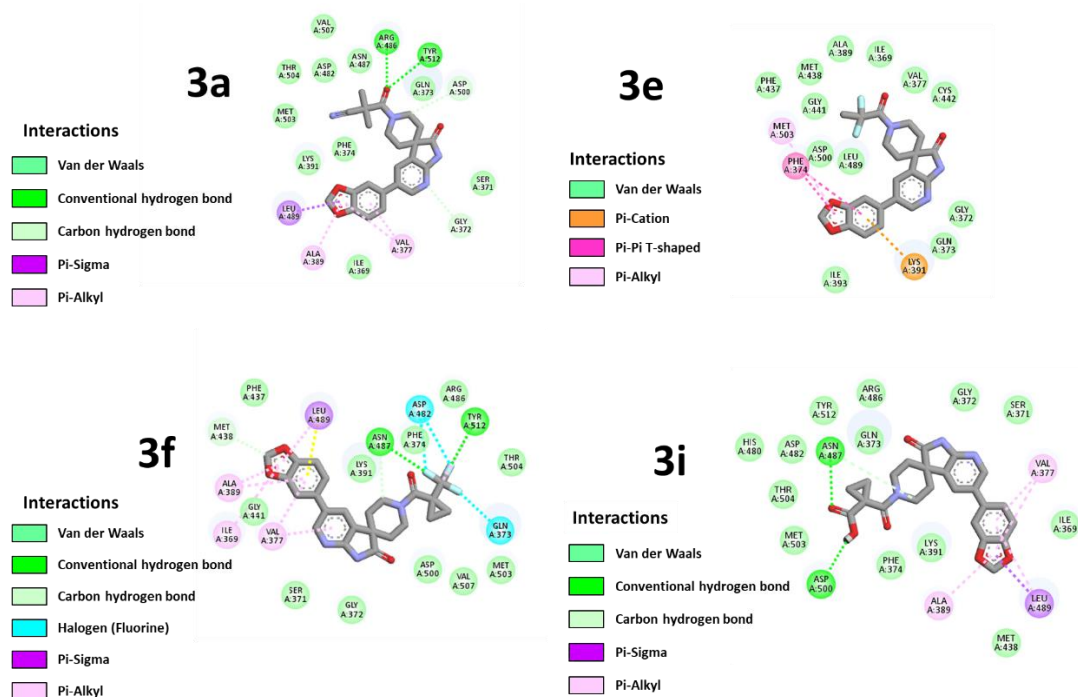


Figure 2. 2D Ligand interaction diagrams for docked compound **3a**, **3e**, **3f** and **3i**.

In vitro anti-cancer activity

The cytotoxic activity of all 12 azaspirooxindolinone derivatives was assessed in a panel of cancer and non-cancer cell lines (**Table 2**). The panel comprises of the following cell lines: A549(human lung adenocarcinoma), HCT116 (human colorectal carcinoma), U2OS (human osteosarcoma), Jurkat (human T lymphocyte), CCRF-CEM (human T-cell leukemia), Ramos (human B-lymphocyte), K562 (human myeloid leukemia), BJ (human foreskin fibroblast) and MRC-5 (human lung fibroblast). Ramos and K562 cells express several significant B-cell-specific markers, including BTK, whereas Jurkat and CCRF-CEM cells are specific for ITK expression¹⁸. All synthesized derivatives were inactive against non-cancer cell lines. Compound **3c** ($IC_{50} = 29.24 \pm 7.57 \mu M$) showed moderate activity against Jurkat cells, with no activity against Ramos or K562 cells. The cytotoxic activity of **3e** was specific to ITK-positive Jurkat ($IC_{50} = 10.85 \pm 1.48 \mu M$) and CCRF-CEM ($IC_{50} = 20.72 \pm 2.67 \mu M$) cells, whereas **3g** ($IC_{50} = 1.42 \pm 0.13 \mu M$) activity was specific to BTK-high Ramos cells. Other compounds, like **3a**, **3d**, **3f**, and **3j** showed high-to-moderate activity in Jurkat, CCRF-CEM, and Ramos cells, indicating their possible dual activity against ITK and BTK. Only **3k** ($IC_{50} = 13.45 \pm 3.02 \mu M$) showed moderate activity against CCRF-CEM cells. Among the active compounds effective against ITK- or BTK-positive cancer cells, only compound **3j**

($IC_{50} = 18.86 \pm 3.34 \mu\text{M}$) exhibited moderate cytotoxicity against ITK/BTK-null U2OS cells.

Our SAR investigations began with the synthesis of 5'-(benzo[d][1,3]dioxol-5-yl)-1-(1-fluorocyclopropane-1-carbonyl)spiro[piperidine-4,3'-pyrrolo[2,3-b]pyridin]-2'(1'H)-one (**I**)¹⁴. The initial evaluation involved replacing the fluorine atoms with small functional groups. Substitution with $-\text{CF}_3$ and $-\text{CN}$ groups yielded compounds **3f** and **3g**, respectively. These compounds exhibited high cytotoxic effects (**3f**, $IC_{50} = 1.82 \pm 0.48 \mu\text{M}$ and **3g**, $IC_{50} = 1.42 \pm 0.13 \mu\text{M}$), showing approximately a 20-fold increase compared to **I**, against RAMOS cells. However, the introduction of a hydroxyl ($-\text{OH}$) group (**3h**) and carboxylic acid ($-\text{COOH}$) group (**3i**) resulted in decreased activity ($IC_{50} > 50 \mu\text{M}$) against RAMOS. Notably, the cytotoxic activity of compound **3f** decreased in ITK cell lines (CCRF-CEM, $IC_{50} = 19.49 \pm 3.74 \mu\text{M}$ and Jurkat, $IC_{50} = 29.41 \pm 5.03 \mu\text{M}$).

Subsequent SAR investigations focused on gem-dimethyl compound 5'-(benzo[d][1,3]dioxol-5-yl)-1-(2-fluoro-2-methylpropanoyl)spiro[piperidine-4,3'-pyrrolo[2,3-b]pyridin]-2'(1'H)-one (**II**)¹⁴. Replacing one methyl of the gem-dimethyl group with a more electronegative atom such as fluorine (**3d**) prominently increased potency (~ 5 fold increase vs **II**; $IC_{50} = 3.06 \pm 0.91 \mu\text{M}$) against RAMOS cells, with a slight drop in cytotoxic effect ($IC_{50} = 3.58 \pm 0.36 \mu\text{M}$) against Jurkat cells. Substituting the fluorine atom with the $-\text{CN}$ group yielded **3a**, which displayed increased activity ITK and BTK cell lines (RAMOS, $IC_{50} = 10.11 \pm 2.13 \mu\text{M}$; CCRF-CEM, $IC_{50} = 19.49 \pm 3.74$; and Jurkat, $IC_{50} = 29.41 \pm 5.03 \mu\text{M}$).

Interestingly, substituting cyclopropyl/gem-dimethyl with an alkene ($=\text{CH}_2$) group (**3j**, $IC_{50} = 1.38 \pm 0.51 \mu\text{M}$) resulted in a similar improvement in potency as **3g** and **3f** in RAMOS cells. These compounds also exhibited high anticancer effects against ITK cell lines (Jurkat, $IC_{50} = 4.16 \pm 0.66 \mu\text{M}$ and CCRF-CEM, $IC_{50} = 14.06 \pm 2.00 \mu\text{M}$).

Introducing an α , β -unsaturated methylene ($-\text{C}=\text{CH}_2$) group (**3k**) in place of the fluoro cyclopropyl group/fluoro gem-dimethyl group of active compounds **I** and **II** led to moderate anti-cancer activity ($IC_{50} = 13.45 \pm 2.00 \mu\text{M}$) in CCRF-CEM cells. The negative result ($IC_{50} > 50 \mu\text{M}$) of **3b** and **3h** indicates that other factors affect hydrogen bonding after introducing a hydroxy group in place of fluorine atoms of **I** and **II**.

Table 2. Cytotoxicity of azaspirooxindolinone derivatives (IC₅₀ values of compounds are in μM). Data are mean \pm SD, $n \geq 6$.

Cmpd	ITK/BTK null			ITK positive		BTK positive		Non-cancer	
	A549	HCT116	U20S	Jurkat	CCRF-CEM	Ramos	K562	MRC-5	BJ
3a	>50	>50	>50	9.36 \pm 0.49	14.33 \pm 2.06	10.11 \pm 2.13	>50	>50	>50
3b	>50	>50	>50	>50	>50	>50	>50	>50	>50
3c	>50	>50	>50	29.24 \pm 7.57	>50	>50	>50	>50	>50
3d	>50	>50	>50	3.58 \pm 0.36	17.24 \pm 3.50	3.06 \pm 0.91	>50	>50	>50
3e	>50	>50	>50	10.85 \pm 1.48	20.72 \pm 2.67	>50	>50	>50	>50
3f	>50	>50	>50	29.41 \pm 5.03	19.49 \pm 3.74	1.82 \pm 0.48	>50	>50	>50
3g	>50	>50	>50	50 \pm 0	>50	1.42 \pm 0.13	>50	>50	>50
3h	>50	>50	>50	>50	>50	>50	>50	>50	>50
3i	>50	>50	>50	>50	>50	>50	>50	>50	>50
3j	>50	>50	18.86 \pm 3.34	4.16 \pm 0.66	14.06 \pm 2.00	1.38 \pm 0.51	>50	>50	>50
3k	>50	>50	>50	>50	13.45 \pm 3.02	>50	>50	>50	>50
3l	>50	>50	>50	>50	>50	>50	>50	>50	>50

Conclusion

In this study, we report the synthesis of new azaspirooxindolinone derivatives and their cytotoxic activity in ITK/BTK-negative and -positive cancer cell lines. A molecular docking score was conducted using AutoDock Vina, and the molecular interactions were evaluated and compared to those of Ibrutinib, which exhibited a binding energy of -9.2 kcal/mol. Compound **3e** exhibited the most favorable docking score of -9.7 kcal/mol, while compounds **3a**, **3f**, **3g**, and **3i** displayed docking scores of 9.4 kcal/mol. The recovery and use of compounds exhibiting robust interactions can be employed to ascertain their efficacy as possible inhibitors of ITK.

Cytotoxicity tests were conducted to investigate the anti-cancer properties of these derivatives. Among all the compounds active in ITK- and BTK-positive cancer cells, only **3j** showed moderate cytotoxicity against ITK/BTK-null U20S cells. Compound **3d** demonstrated the highest cytotoxicity among all the synthesized derivatives against

Jurkat cells and was also highly active against RAMOS cells. Compound **3j** exhibited the highest cytotoxicity against RAMOS cells, but this compound was also highly active against Jurkat cells. **3c** and **3g** were specifically cytotoxic to Jurkat and Ramos cells, respectively.

Most compounds that demonstrated activity in RAMOS cells did not exhibit cytotoxic effects in K562 cells. This lack of cytotoxicity in K562 cells is likely attributed to their low levels of BTK expression, possibly due to the presence of the BCR-ABL fusion gene, a recognized primary driver in K562 cells²¹. Nevertheless, none of the active compounds exhibited cytotoxic effects against non-cancer cell lines. Further investigations are required to determine the specificity of the compounds against members of the Tec Family.

Experimental Section

Chemistry

Materials and Methods

The chemicals used in this study were obtained from reputable suppliers, including Lancaster (Alfa Assar, Johnson Matthey Co, Ward Hill, MA, USA), Sigma-Aldrich (St Louis, MO, USA), and Spectrochem Pvt. Ltd (Mumbai, India). The aryl boronic acids were obtained from Combi-Blocks, Inc., San Diego, CA, USA. The reactions were seen using thin-layer chromatography (TLC) on an aluminum TLC plate coated with silica gel containing the fluorescent indication F254S. The TLC plates were visualized using ultraviolet (UV) light, KMnO₄ stain, and an iodine indicator. The ¹H NMR and ¹³C NMR spectra were acquired using an Agilent 400 MHz NMR Magnet manufactured by Agilent Technologies, Incorporated, located in Santa Clara, CA, USA. The chemical changes were quantified in parts per million (ppm) relative to an internal tetramethylsilane (TMS) standard, exhibiting a downfield shift. The spectral patterns were classified as follows: s, representing a singlet; d, representing a doublet; dd, representing a double doublet; t, representing a triplet; td, representing a triplet of doublet; bs, representing a wide singlet; and m, representing a multiplet. The ESI spectra were obtained using the micro mass, Quattro LC instrument, and the ESI+ software. The capillary voltage applied was 3.98 kV, and the ESI mode positive ion

trap detector was employed. The infrared spectra were obtained using an FT-IR spectrometer, and only the significant peaks were documented in units of cm⁻¹. All solutions were made using deionized distilled water. All additional reagents utilized in this study were of standard quality and obtained from commercial sources.

Synthesis of 5'-(benzo[d][1,3]dioxol-5-yl)spiro[piperidine-4,3'-pyrrolo[2,3-b]pyridin]-2'(1'H)-one (1d)¹⁵: Yield: 90%, MP: 260-264 °C, White solid, FT- IR (KBr): ν_{max} 3778, 3605, 3153, 1717, 1611, 1457, 1220, 1038, 810, 688 cm⁻¹. ¹H-NMR (400 MHz, CDCl₃): δ 8.27 (d, J = 1.6 Hz, 1H), 7.81 (d, J = 1.6 Hz, 1H), 6.96-6.99 (m, 2H), 6.89-6.91 (m, 1H), 6.02 (s, 2H), 3.36-3.42 (m, 2H), 3.08-3.14 (m, 2H), 1.96-2.02 (m, 2H), 1.78-1.84 (m, 2H). ¹³C NMR, (100 MHz, DMSO-d₆): δ 28.32, 43.59, 101.19, 107.17, 108.72, 120.21, 127.23, 129.48, 130.18, 131.59, 144.66, 146.89, 148.02, 155.00, 179.69. LC-MS ESI: m/z = 324.30 (M+H)⁺.

General procedure for the synthesis of compounds (3a-3i): To a solution of acid (1.0 equiv.), HATU (1.5 equiv.) and DIPEA (3.0 equiv.) in DMF (0.2 M) were added to the corresponding amine (1.2 equiv.) at room temperature. The reaction mixture was stirred at ambient temperature for 2 h. The reaction mixture was poured onto ice-cold water and stirred for 15 min. The resulting precipitated solid compound was collected by filtration, washed with water, and dried to obtain a crude compound. The crude compound was purified by GRACE flash chromatography using a C18, 12 g column with 0.1% formic acid in water and acetonitrile as an eluent to give the final compound.

3-(5'-(Benzo[d][1,3]dioxol-5-yl)-2'-oxo-1',2'-dihydrospiro[piperidine-4,3'-pyrrolo[2,3-b]pyridin]-1-yl)-2,2-dimethyl-3-oxopropanenitrile (3a): Yield: 40%; Melting point: 258 °C; Physical state: White solid; ¹H-NMR (400 MHz, DMSO-d₆): δ 11.16 (s, 1H), 8.35 (s, 1H), 8.18 (s, 1H), 7.33 (s, 1H), 7.19 (d, J = 8.0 Hz, 1H), 6.99 (d, J = 8.0 Hz, 1H), 6.05 (s, 2H), 3.98-4.02 (m, 4H), 1.87-1.96 (m, 4H), 1.58 (m, 6H); ¹³C NMR (125 MHz, DMSO-d₆): δ 24.98, 24.98, 34.38, 35.47, 35.47, 45.21, 110.09, 107.07, 108.59, 120.08, 122.09, 127.98, 129.64, 129.96, 131.53, 144.15, 146.74, 147.93, 154.92, 165.48, 180.21; FT- IR (KBr): ν (-C-O): 1375 cm⁻¹; ν (-C-H bending for methylene): 1454 cm⁻¹; ν (-C=O for amide): 1629, 1724 cm⁻¹; ν (-NH for amine): 3450 cm⁻¹. (-CN peak was not observed); LC-MS (ESI) m/z: 419.2 [M+H]⁺.

5'-(Benzo[d][1,3]dioxol-5-yl)-1-(2-hydroxy-2-methylpropanoyl)spiro[piperidine-4,3'-pyrrolo[2,3-b]pyridin]-2'(1'H)-one (3b): Yield: 51%; Melting point: 245 °C; Physical state: White solid; ¹H-NMR (400 MHz, DMSO-d₆): δ 11.15 (s, 1H), 8.34 (d, J = 1.2 Hz, 1H), 8.14 (d, J = 1.2 Hz, 1H), 7.31 (d, J = 0.8 Hz, 1H), 7.18 (d, J = 8.0 Hz, 1H), 6.99 (d, J = 8.0 Hz, 1H), 6.05 (s, 2H), 4.15-3.80 (m, 4H), 1.96-1.75 (m, 4H), 1.62 (s, 3H), 1.57 (s, 3H); ¹³C NMR (105 MHz, DMSO-d₆): δ 12.76, 14.56, 31.20, 45.14, 101.08, 107.02, 108.59, 120.04, 120.18, 127.97, 129.60, 129.96, 131.55, 144.16, 146.74, 147.93, 154.92, 162.61, 180.19; FT- IR (KBr): ν(-C-O): 1033 cm⁻¹; ν(-C-N stretching for aromatic amine): 1373 cm⁻¹; ν(-C-O bending for methylene): 1463 cm⁻¹; ν(-C=O for amide): 1614, 1707 cm⁻¹; ν(-OH for alcohol): 3552 cm⁻¹; LC-MS (ESI) m/z: 408.20 [MH]⁺.

Ethyl 3-(5'-(benzo[d][1,3]dioxol-5-yl)-2'-oxo-1',2'-dihydrospiro[piperidine-4,3'-pyrrolo[2,3-b]pyridin]-1-yl)-2,2-dimethyl-3-oxopropanoate (3c): Yield: 22%; Melting point: 247 °C; Physical state: White solid; ¹H-NMR (500 MHz, DMSO-d₆): δ 11.15 (s, 1H), 8.33 (d, J = 2.4 Hz, 1H), 8.07 (d, J = 2.0 Hz, 1H), 7.33 (d, J = 1.6 Hz, 1H), 7.17 (dd, J = 1.6, 8.0 Hz, 1H), 6.99 (d, J = 8.0 Hz, 1H), 6.05 (s, 2H), 4.15 (q, J = 6.8 Hz, 2H), 3.93-3.36 (m, 4H), 1.80-1.75 (m, 4H), 1.36 (s, 6H), 1.23 (t, J = 6.8 Hz, 3H); ¹³C NMR (125 MHz, DMSO-d₆): δ 28.42, 28.42, 40.15, 40.15, 43.47, 55.48, 55.59, 110.47, 112.25, 118.84, 127.33, 129.57, 130.14, 130.41, 144.63, 148.57, 149.16, 154.86, and 179.76; FT- IR (KBr) : ν(-C-O for ester): 1031 cm⁻¹; ν(-C-O for ester): 1223 cm⁻¹; ν(-C-N stretching for aromatic amine): 1375 cm⁻¹; ν(-C-O bending for methylene): 1462 cm⁻¹; ν(-C=O for lactum): 1649 cm⁻¹, ν(-C=O for ester): 1718 cm⁻¹; LC-MS (ESI) m/z: 466.20 [M+H]⁺.

5'-(Benzo[d][1,3]dioxol-5-yl)-1-(2,2-difluoropropanoyl)spiro[piperidine-4,3'-pyrrolo[2,3-b]pyridin]-2'(1'H)-one (3d): Yield: 56%; Melting point: 262 °C; Physical state: White solid; ¹H-NMR (500 MHz, DMSO-d₆): δ 8.30 (d, J = 1.6 Hz, 1H), 8.07 (s, 1H), 7.62 (d, J = 2.0 Hz, 1H), 6.97-6.89 (m, 3H), 6.02 (s, 2H), 4.26-4.14 (m, 3H), 3.90-3.88 (m, 1H), 1.99-1.84 (m, 7H); ¹³C NMR (125 MHz, DMSO-d₆): δ 21.96 (t, J = 24.8 Hz), 31.18, 31.11, 45.07, 101.07, 107.04, 108.56, 120.03, 127.91, 129.62, 129.95, 131.50, 144.13, 146.73, 147.92, 154.88, 161.28 (t, J = 28.8 Hz), 180.17; LC-MS (ESI) m/z: 416.2 [M+H]⁺.

5'-(Benzo[d][1,3]dioxol-5-yl)-1-(2,2,2-trifluoroacetyl)spiro[piperidine-4,3'-pyrrolo[2,3-b]pyridin]-2'(1'H)-one (3e): Yield: 51%; Melting point: 242 °C; Physical state: White solid; ¹H-NMR (500 MHz, DMSO-d₆): δ 8.30 (d, J = 6.0 Hz, 1H), 8.05 (brs, 1H), 7.59 (d, J = 2.0 Hz, 1H), 6.97-6.89 (m, 3H), 6.02 (s, 2H), 4.37-4.33 (m, 1H), 4.17-4.15 (m, 1H), 3.94-3.91 (m, 2H), 2.05-1.97 (m, 4H); ¹³C NMR (125 MHz, DMSO-d₆): δ 30.94, 31.85, 44.82, 101.11, 106.97, 108.63, 117 (d, J = 185.6 Hz), 127.89, 129.55, 129.77, 131.59, 144.20, 146.73, 147.93, 154.17, 155 (d, J = 50.8 Hz), 180.53; FT- IR (KBr): ν(-C-O): 1215 cm⁻¹; ν(-C-N stretching for aromatic amine): 1375 cm⁻¹; ν(-C-H bending for methylene): 1462 cm⁻¹; ν(-C=O for amide): 1699 cm⁻¹; ν(-NH for amine): 3458 cm⁻¹; LC-MS (ESI) m/z: 420.0 [M+H]⁺.

5'-(Benzo[d][1,3]dioxol-5-yl)-1-(1-(trifluoromethyl)cyclopropane-1-carbonyl)spiro[piperidine-4,3'-pyrrolo[2,3-b]pyridin]-2'(1'H)-one (3f): Yield: 62%; Melting point: 245 °C; Physical state: White solid; ¹H-NMR (500 MHz, DMSO-d₆): δ 8.30 (d, J = 2.0 Hz, 1H), 7.92 (s, 1H), 7.60 (s, 1H), 6.98-6.9 (m, 3H), 6.02 (s, 2H), 4.18-3.86 (m, 4H), 3.02-1.90 (m, 4H), 1.38-1.36 (m, 2H), 1.23-1.21 (m, 2H); ¹³C NMR (125 MHz, DMSO-d₆): δ 9.83, 26.62, 26.88, 31.44, 45.14, 101.13, 107.08, 108.64, 120.10, 124.40, 126.57, 127.99, 129.69, 129.97, 131.61, 144.18, 146.77, 147.96, 154.96, 162.80, 180.25; FT- IR (KBr): ν(-C-N stretching for aromatic amine): 1375 cm⁻¹; ν(-C-H bending for methylene): 1462 cm⁻¹; ν(-C=O for lactum): 1647 cm⁻¹; ν(-C=O for amide): 1722 cm⁻¹; ν(-NH for amine): 3500 cm⁻¹; LC-MS (ESI) m/z: 460.20 [M+H]⁺.

1-(5'-(Benzo[d][1,3]dioxol-5-yl)-2'-oxo-1',2'-dihydrospiro[piperidine-4,3'-pyrrolo[2,3-b]pyridine]-1-carbonyl)cyclopropane-1-carbonitrile (3g): Yield: 59%; Melting point: 267 °C; Physical state: White solid; ¹H-NMR (400 MHz, CDCl₃): δ 8.30 (d, J = 1.6 Hz, 1H), 8.03 (s, residual formic acid from purification, 1H), 7.62 (d, J = 2.0 Hz, 1H), 6.98-6.89 (m, 3H), 6.02 (s, 2H), 4.25-4.23 (m, 3H), 3.86-3.84 (m, 1H), 2.06-1.80 (m, 4H), 1.57-1.56 (m, merged in CDCl₃ moisture, 4H); ¹³C NMR (125 MHz, DMSO-d₆): δ 28.50, 28.50, 31.87, 31.87, 45.47, 73.14, 101.06, 107.10, 108.58, 120.10, 128.40, 129.52, 129.90, 131.63, 144.06, 146.72, 147.92, 154.93, 173.33, 180.43; FT- IR (KBr): ν(-C-N stretching for aromatic amine): 1375 cm⁻¹; ν(-C-H bending for methylene): 1467 cm⁻¹; ν(-C=O for lactum): 1656 cm⁻¹; ν(-C=O for amide): 1712 cm⁻¹; ν(-NH for amine): 3512 cm⁻¹; LC-MS (ESI) m/z: 417.20 [M+H]⁺.

5'-(Benzo[d][1,3]dioxol-5-yl)-1-(1-hydroxycyclopropane-1-carbonyl)spiro

[piperidine-4,3'-pyrrolo[2,3-b]pyridin]-2'(1'H)-one (3h): Yield: 34%; Melting point: 165 °C; Physical state: White solid; ¹H-NMR (500 MHz, DMSO-d₆): δ 11.13 (s, 1H), 8.33 (d, J = 2.0 Hz, 1H), 8.10 (d, J = 2.0 Hz, 1H), 7.33 (d, J = 1.6 Hz, 1H), 7.18 (dd, J = 1.6, 8.0 Hz, 1H), 6.99 (d, J = 8.4 Hz, 1H), 6.35 (s, 1H), 6.05 (s, 2H), 4.15-3.78 (m, 4H), 1.82-1.78 (m, 4H), 0.99-0.98 (m, 2H), 0.79-0.78 (m, 2H); FT- IR (KBr) ν(-C-H bending for methylene): 1467 cm⁻¹; ν(-C=O for lactum): 1610 cm⁻¹; ν(-C=O for amide): 1720 cm⁻¹; ν(-OH for alcohol): 3404 cm⁻¹; LC-MS (ESI) m/z: 408.20 [M+H]⁺.

1-(5'-(Benzo[d][1,3]dioxol-5-yl)-2'-oxo-1',2'-dihydrospiro[piperidine-4,3'-pyrrolo

[2,3-b]pyridine]-1-carbonyl)cyclopropane-1-carboxylic acid (3i): Yield: 21% (over two steps); Melting point: 267 °C; Physical state: White solid; ¹H-NMR (500 MHz, DMSO-d₆): δ 12.85 (brs, 1H), 11.13 (s, 1H), 8.33 (d, J = 2.0 Hz, 1H), 8.04 (d, J = 1.6 Hz, 1H), 7.30 (s, 1H), 7.16 (dd, J = 1.2, 6.4 Hz, 1H), 6.99 (d, J = 6.4 Hz, 1H), 6.05 (s, 2H), 3.93-3.76 (m, 4H), 1.88-1.78 (m, 4H), 1.41-1.21 (m, 4H); FT- IR (KBr): ν(-C-N stretching for aromatic amine): 1373 cm⁻¹; ν(-C-H bending for methylene): 1462 cm⁻¹; ν(-C=O for lactum): 1608 cm⁻¹; ν(-C=O for amide): 1718 cm⁻¹; ν(-COOH): 3458 cm⁻¹; LC-MS (ESI) m/z: 436.20 [M+H]⁺.

5'-(Benzo[d][1,3]dioxol-5-yl)-1-(2-fluoroacryloyl)spiro[piperidine-4,3'-pyrrolo[2,3-b]pyridin]-2'(1'H)-one (3j): To a solution of compound **1d** (70 mg, 1.0 equiv.), 2-fluoroacrylic acid (2.5 equiv.), DIPEA (5.0 equiv.) in DMF (2.0 mL) was added to T₃P (50% in EtOAc, 5.0 equiv.) at ambient temperature and stirred for 2h. The reaction mixture was poured onto ice-cold water and extracted with ethyl acetate. The combined extracts were washed with water and brine, dried over anhydrous sodium sulphate and concentrated to obtain a crude compound. This was purified by GRACE flash chromatography using 0.1% formic acid in water and acetonitrile as an eluent to afford the title compound as a white solid.

Yield: 47%; Melting point: 269 °C; Physical state: White solid; ¹H-NMR (500 MHz, DMSO-d₆): δ 11.16 (s, 1H), 8.35 (d, J = 2.0 Hz, 1H), 8.17 (d, J = 2.0 Hz, 1H), 7.33 (d, J = 1.6 Hz, 1H), 7.19 (dd, J = 1.6, 8.0 Hz, 1H), 6.99 (d, J = 8.0 Hz, 1H), 6.05 (s, 2H), 5.33-5.16 (m, 2H), 3.95-3.87 (m, 4H), 1.92-1.84 (m, 4H); ¹³C NMR (125 MHz, DMSO-d₆): δ 38.87, 39.07, 39.28, 39.50, 39.71, 39.92, 40.12, 45.25, 98.47, 98.61,

101.16, 107.08, 108.67, 120.09, 128.00, 129.74, 129.99, 131.58, 144.20, 146.80, 148.00, 154.83, 154.97, 157.48, 160.30, 160.61 and 180.28; FT- IR (KBr): ν (-C-N stretching for aromatic amine): 1226 cm^{-1} ; ν (-C-H bending for methylene): 1460 cm^{-1} ; ν (-C=C for alkene): 1637 cm^{-1} ; ν (-C=O for lactum): 1660 cm^{-1} ; ν (-C=O for amide): 1714 cm^{-1} ; ν (-C-H stretching for alkene): 3113 cm^{-1} ; ν (-NH): 3446 cm^{-1} ; LC-MS (ESI) m/z : 396.20 $[\text{M}+\text{H}]^+$.

1-Acryloyl-5'-(benzo[d][1,3]dioxol-5-yl)spiro[piperidine-4,3'-pyrrolo[2,3-b]pyridin]-2'(1'H)-one (3k): To a solution of compound **1d** (70 mg, 1.0 equiv.), DIPEA (10.0 equiv.) in THF (4.0 mL) at 0°C were added acryloyl chloride (1.0 equiv.) and the resulting reaction mixture was stirred at the same temperature for 5 min. The reaction mixture was poured onto ice-cold water and extracted with ethyl acetate. The combined extracts were washed with water, and brine, dried over anhydrous sodium sulphate and concentrated to obtain crude compound, which upon purification by GRACE flash chromatography using 0.1% formic acid in water and acetonitrile as an eluent to afford the title compound as a white solid.

Yield : 49%; Melting point: 242 °C; Physical state: White solid; $^1\text{H-NMR}$ (500 MHz, DMSO-d_6): δ 11.12 (s, 1H), 8.34 (d, $J = 2.0$ Hz, 1H), 8.17 (d, $J = 2.0$ Hz, 1H), 7.33 (d, $J = 1.6$ Hz, 1H), 7.19 (dd, $J = 1.6, 8.0$ Hz, 1H), 6.98 (d, $J = 8.0$ Hz, 1H), 6.88 (dd, $J = 10.4, 17.6$ Hz, 1H), 6.15 (dd, $J = 2.4, 16.8$ Hz, 1H), 6.05 (s, 2H), 5.71 (dd, $J = 2.0, 10.4$ Hz, 1H), 3.95-3.87 (m, 4H), 1.90-1.74 (m, 4H); $^{13}\text{C NMR}$ (125 MHz, DMSO-d_6): δ 31.43, 32.30, 37.05, 40.81, 45.34, 101.14, 107.08, 108.65, 120.06, 127.19, 128.27, 128.52, 129.66, 129.93, 131.59, 144.11, 146.77, 147.98, 154.98, 164.44, and 180.40; FT- IR (KBr): ν (-C-N stretching for aromatic amine): 1232 cm^{-1} ; ν (-C-H bending for methylene): 1462 cm^{-1} ; ν (-C=C for alkene): 1575 cm^{-1} ; ν (-C=O for lactum): 1600 cm^{-1} ; ν (-C=O for amide): 1724 cm^{-1} ; ν (-C-H stretching for alkene): 3086 cm^{-1} ; ν (-NH): 3427 cm^{-1} ; LC-MS (ESI) m/z : 378.62 $[\text{M}+\text{H}]^+$.

5'-(Benzo[d][1,3]dioxol-5-yl)-1-((trifluoromethyl)sulfonyl)spiro[piperidine-4,3'-pyrrolo[2,3-b]pyridin]-2'(1'H)-one (3l): To a solution of compound **1d** (60 mg, 1.0 equiv.), TEA (5.0 equiv.), in dichloromethane (2.0 mL) was added triflic anhydride (1.5 equiv.) at 0°C, and the resulting reaction mixture was stirred at the same temperature for 2h. The reaction mixture was quenched by adding saturated NaHCO_3 solution and extracted with dichloromethane. The combined extracts were washed with

water, and brine, dried over anhydrous sodium sulfate, and concentrated to obtain a crude compound, which upon purification by GRACE flash chromatography using 0.1% formic acid in water and acetonitrile as an eluent to afford the title compound as an off-white solid.

Yield: 42%; Melting point: 302 °C; Physical state: White solid; ¹H-NMR (500 MHz, DMSO-d₆): δ 11.23 (s, 1H), 8.36 (s, 1H), 8.19 (s, 1H), 7.33 (d, J = 1.5 Hz, 1H), 7.20 (dd, J = 2.0, 8.0 Hz, 1H), 7.01 (d, J = 8.0 Hz, 1H), 6.06 (s, 2H), 3.81-3.84 (m, 4H), 1.91-2.07 (m, 4H); ¹³C NMR (125 MHz, DMSO-d₆): δ 31.32, 42.18, 43.97, 101.18, 107.10, 108.70, 120.11, 127.53, 129.78, 130.10, 131.55, 144.39, 146.83, 148.01, 154.95, and 179.95; FT- IR (KBr): ν(-S=O for sulfonamide): 1380 cm⁻¹; ν(-C-H bending for methylene): 1467 cm⁻¹; ν (-C=O for lactum): 1604 cm⁻¹; ν (-C=O for amide): 1710 cm⁻¹; ν (-NH₂): 3452 cm⁻¹; LC-MS (ESI) m/z: 456.0 [M+H]⁺.

1-(2,2-Difluoropropanoyl)-5'-(3,4,5-trimethoxyphenyl)spiro[piperidine-4,3'-pyrrolo[2,3-b]pyridin]-2'(1'H)-one (3m): Yield: 41%; Melting point: 210 °C; Physical state: White solid; ¹H-NMR (500 MHz, DMSO-d₆): δ 8.43 (d, J = 2.0 Hz, 1H), 8.16 (d, J = 2.0 Hz, 1H), 6.91 (s, 2H), 3.87 (s, 6H), 3.80-4.08 (m, 4H), 3.68 (s, 3H), 1.86-1.94 (m, 4H), 1.85 (t, J = 20.0 Hz, 3H); FT- IR (KBr): ν(-C-O): 1122 cm⁻¹; ν (-C-H bending for methylene): 1473 cm⁻¹; ν (-C=O for lactum): 1660 cm⁻¹; ν (-C=O for amide): 1718 cm⁻¹; ν (-NH for amine): 3493 cm⁻¹; LC-MS (ESI) m/z: 425.2 [M+H]⁺.

Computational Section

Preparation of Protein/Receptor

The crystallographic arrangement of the BTK complex in association with the inhibitor Ibrutinib, identified by the PDB ID- 5P9J²¹, was obtained from the Research Collaboratory for Structural Bioinformatics (RCSB), a renowned protein data bank database (www.rcsb.org). The downloaded file was in .pdb format and possessed a resolution of 2.5 Å. The protein was generated via the AutoDock software¹⁸. The study focused on a single chain that was selected as the subject of investigation. The crystal structure was devoid of its native ligand, non-interacting ions, and water molecules. Efficient hydrogen atoms were incorporated to alleviate the stress on the crystal lattice and render the protein amenable for utilization in the AutoDock docking simulation tool. The protein was generated utilizing the UCSF Chimera graphical user interface

after performing structural reduction procedures, such as the inclusion of hydrogen atoms, Gasteiger charge calculations, and the consolidation of non-polar hydrogens with carbon atoms.

Chemsketch

ChemSketch is a program designed specifically for creating sketches of chemical structures while concentrating on chemical structure data. It helps with two-dimensional compound drawing, which can then be swiftly converted into three dimensions utilizing a three-dimensional algorithm that also considers the molecular dynamics of such compounds. It is widely used in the fields of cheminformatics and bioinformatics. Analogues of the compounds have been made using ChemSketch. Ligand input files for docking were prepared using UCSF Chimera and stored in the mol2 file format²².

Chimera

Utilizing UCSF Chimera, the interactions were studied and visualized. It is software that can be expanded to analyze molecular structures as well as related data like density maps, results of sequence alignment, results of docking, conclusions from trajectory analysis, etc. Along with the essential features like visualization and expansion, it also provides a very high level of functionality²³.

Discovery Studio

The Discovery Studio software facilitates the identification of the many forms of interactions and bond lengths that occur between the active sites in both the target and ligand conformations. Discovery Studio is a comprehensive and integrated graphical interface that facilitates efficient drug design and protein modeling²⁴.

Docking

The molecular docking method was applied to the selected ligands with the help of AutoDock Vina²⁵. A grid box for ITK with the dimensions X: 2.866, Y: 8.84, Z: 14.89 Å, and the size of the grid box- 22 × 22 × 22, was identified as the protein target docking site and the best molecular interacting compounds were observed. The interactions between the active sites in the target and ligand conformation, along with

the type of interaction and bond distances, were identified using Discovery Studio Visualizer.

Biology

Cell lines

Cells were purchased from ATCC (Middlesex, UK) and DSMZ (Braunschweig, Germany) and maintained at 37°C in a humidified incubator (5% CO₂/atmospheric air) in recommended growth medium supplemented with 10% fetal calf serum, antibiotics (100 mg/mL streptomycin and 100 U/mL penicillin), 2 mM glutamine, 1 mM NaHCO₃, 1 mM C₃H₃NaO₃, and 20 mM HEPES. Cell lines were validated monthly and regularly checked for mycoplasma contamination every 2 weeks.

Cytotoxicity assay

The cytotoxicity of compounds was determined using an MTS assay protocol developed for routine compound screening at our facility, and IC₅₀ values were calculated as described previously¹⁸.

DECLARATION OF COMPETING INTEREST

The authors declare no conflicting interest.

DATA AVAILABILITY STATEMENT

All data supporting the findings of this study are available in the manuscript or supplementary files. Cytotoxicity data of compounds are stored in the IMTM Dotmatics database, and available from the corresponding author (V. Das) upon reasonable request.

ACKNOWLEDGEMENTS

Dr. Rambabu Gundla acknowledges GITAM for financial assistance and facility. GR, RN, and RG thank Aragen Lifesciences Pvt Ltd. Hyderabad, India, for providing computational resources for synthesizing and characterizing all the compounds by NMR, LC-MS, and FT-IR. All biological part of the study was supported in parts by the infrastructural projects (CZ-OPENSREEN – LM2023052; EATRIS-CZ – LM2023053), the projects National Institute for Cancer Research (Program EXCELES, ID Project No. LX22NPO5102) - Funded by the European Union - Next Generation

EU from the Ministry of Education, Youth and Sports of the Czech Republic (MEYS), project TN02000109 (Personalized Medicine: From Translational Research into Biomedical Applications is co-financed with the state support of the Technology Agency of the Czech Republic as part of the National Centers of Competence Program), and project SALVAGE (registration number: CZ.02.01.01/00/22_008/0004644, supported by OP JAK, with co-financing from the EU and the State Budget).

Supplementary Information

Supporting Information contains the characterization of all compounds (^1H NMR, ^{13}C NMR, HPLC, and FT-IR spectra).

References

1. Shoji K, Suzuki A, Okamoto M, Tsinda EK, Sugawara N, Sasaki M, Nogami Y, Kobayashi M, Oshitani H, Yanai M. Prolonged shedding of infectious viruses with haplotype switches of SARS-CoV-2 in an immunocompromised patient. *J Infect Chemother.* **2022**, 28, 1001-1004. doi: 10.1016/j.jiac.2022.04.004.
2. Lechner KS, Neurath MF, Weigmann B. Role of the IL-2 inducible tyrosine kinase ITK and its inhibitors in disease pathogenesis. *J Mol Med (Berl).* **2020**, 98, 1385-1395. doi: 10.1007/s00109-020-01958-z.
3. Garg N, Padron EJ, Rammohan KW, Goodman CF. Bruton's Tyrosine Kinase Inhibitors: The Next Frontier of B-Cell-Targeted Therapies for Cancer, Autoimmune Disorders, and Multiple Sclerosis. *J Clin Med.* **2022**, 11, 6139. doi: 10.3390/jcm11206139.
4. Davids MS, Brown JR. Ibrutinib: a first in class covalent inhibitor of Bruton's tyrosine kinase. *Future Oncol.* **2014**, 10, 957-67. doi: 10.2217/fon.14.51.
5. Nadeem A, Ahmad SF, Al-Harbi NO, Ibrahim KE, Siddiqui N, Al-Harbi MM, Attia SM, Bakheet SA. Inhibition of Bruton's tyrosine kinase and IL-2 inducible T-cell kinase suppresses both neutrophilic and eosinophilic airway inflammation in a cockroach allergen extract-induced mixed granulocytic mouse model of asthma using preventative and therapeutic strategy. *Pharmacol Res.* **2019**, 148, 104441. doi: 10.1016/j.phrs.2019.104441.

6. Molina-Cerrillo J, Alonso-Gordoa T, Gajate P, Grande E. Bruton's tyrosine kinase (BTK) as a promising target in solid tumors. *Cancer Treat Rev.* **2017**, 58, 41-50. doi: 10.1016/j.ctrv.2017.06.001.
7. Ran F, Liu Y, Xu Z, Meng C, Yang D, Qian J, Deng X, Zhang Y, Ling Y. Recent development of BTK-based dual inhibitors in the treatment of cancers. *Eur J Med Chem.* **2022**, 233, 114232. doi: 10.1016/j.ejmech.2022.114232.
8. Zhou D, Zuo Y, Pan Z. Discovery of Potent and Highly Selective Interleukin-2-Inducible T-Cell Kinase Degradable with *In Vivo* Activity. *J Med Chem.* **2023**, 66, 4979-4998. doi: 10.1021/acs.jmedchem.2c02078.
9. Wang X, Xue G, Pan Z. Design, synthesis and structure-activity relationship of indolylindazoles as potent and selective covalent inhibitors of interleukin-2 inducible T-cell kinase (ITK). *Eur J Med Chem.* **2020**, 187, 111918. doi: 10.1016/j.ejmech.2019.111918.
10. Ran F, Liu Y, Xu Z, Meng C, Yang D, Qian J, Deng X, Zhang Y, Ling Y. Recent development of BTK-based dual inhibitors in the treatment of cancers. *Eur J Med Chem.* **2022**, 233, 114232. doi: 10.1016/j.ejmech.2022.114232..
11. Norman P. Inducible tyrosine kinase inhibitors: a review of the patent literature (2010 - 2013). *Expert Opin Ther Pat.* **2014**, 24, 979-91. doi: 10.1517/13543776.2014.936381.
12. Ran F, Liu Y, Xu Z, Meng C, Yang D, Qian J, Deng X, Zhang Y, Ling Y. Recent development of BTK-based dual inhibitors in the treatment of cancers. *Eur J Med Chem.* **2022**, 233, 114232. doi: 10.1016/j.ejmech.2022.114232.
13. Dubovsky JA, Beckwith KA, Natarajan G, Woyach JA, Jaglowski S, Zhong Y, Hessler JD, Liu TM, Chang BY, Larkin KM, Stefanovski MR, Chappell DL, Frizzera FW, Smith LL, Smucker KA, Flynn JM, Jones JA, Andritsos LA, Maddocks K, Lehman AM, Furman R, Sharman J, Mishra A, Caligiuri MA, Satoskar AR, Buggy JJ, Muthusamy N, Johnson AJ, Byrd JC. Ibrutinib is an irreversible molecular inhibitor of ITK driving a Th1-selective pressure in T lymphocytes. *Blood.* **2013**, 122, 2539-49. doi: 10.1182/blood-2013-06-507947.
14. Mudasani G, Paidikondala K, Gurská S, Maddirala SJ, Džubák P, Das V, Gundla R. C-5 Aryl Substituted Azaspirooxindolinones Derivatives: Synthesis and Biological Evaluation as Potential Inhibitors of Tec Family Kinases. *Eur J Org Chem.* **2021**, 4630–4640.

15. Mudasani G, Paidikondala K, Gundla R, Maddirala SJ, Das, V. Synthesis and Biological Evaluation of 5'-Arylspiro[piperidine-4,3'-pyrrolo-[2,3- b]pyridin] Analogues. *ChemistrySelect*. **2021**, 6, 3378–3381
16. Herman SE, Gordon AL, Hertlein E, Ramanunni A, Zhang X, Jaglowski S, Flynn J, Jones J, Blum KA, Buggy JJ, Hamdy A, Johnson AJ, Byrd JC. Bruton tyrosine kinase represents a promising therapeutic target for treatment of chronic lymphocytic leukemia and is effectively targeted by PCI-32765. *Blood*. **2011**, 117, 6287-96. doi: 10.1182/blood-2011-01-328484.
17. Marcotte DJ, Liu YT, Arduini RM, Hession CA, Miatkowski K, Wildes CP, Cullen PF, Hong V, Hopkins BT, Mertsching E, Jenkins TJ, Romanowski MJ, Baker DP, Silvian LF. Structures of human Bruton's tyrosine kinase in active and inactive conformations suggest a mechanism of activation for TEC family kinases. *Protein Sci*. **2010**, 19, 429-39. doi: 10.1002/pro.321.
18. Koraboina CP, Maddipati VC, Annadurai N, Gurská S, Džubák P, Hajdúch M, Das V, Gundla R. Synthesis and Biological Evaluation of Oxindole Sulfonamide Derivatives as Bruton's Tyrosine Kinase Inhibitors. *ChemMedChem*. **2024**, 19, e202300511. doi: 10.1002/cmdc.202300511.
19. Wang X, Xue G, Pan Z. Design, synthesis and structure-activity relationship of indolylindazoles as potent and selective covalent inhibitors of interleukin-2 inducible T-cell kinase (ITK). *Eur J Med Chem*. **2020**, 187, 111918. doi: 10.1016/j.ejmech.2019.111918.
20. Mamand S, Allchin RL, Ahearne MJ, Wagner SD. Comparison of interleukin-2-inducible kinase (ITK) inhibitors and potential for combination therapies for T-cell lymphoma. *Sci Rep*. **2018**, 8, 14216. doi: 10.1038/s41598-018-32634-5.
21. Bender AT, Gardberg A, Pereira A, Johnson T, Wu Y, Grenningloh R, Head J, Morandi F, Haselmayer P, Liu-Bujalski L. Ability of Bruton's Tyrosine Kinase Inhibitors to Sequester Y551 and Prevent Phosphorylation Determines Potency for Inhibition of Fc Receptor but not B-Cell Receptor Signaling. *Mol Pharmacol*. **2017**, 91, 208-219. doi: 10.1124/mol.116.107037.
22. A.D. Hunter. ACD/ChemSketch 1.0 (freeware); ACD/ChemSketch 2.0 and its Tautomers, Dictionary, and 3D Plug-ins; ACD/HNMR 2.0; ACD/CNMR 2.0. *J Chem Edu*. **1997**, 74, 905.

23. Pettersen EF, Goddard TD, Huang CC, Couch GS, Greenblatt DM, Meng EC, Ferrin TE. UCSF Chimera--a visualization system for exploratory research and analysis. *J Comput Chem.* **2004**, 25, 1605-12. doi: 10.1002/jcc.20084.
24. Discovery studio. D Studio. Accelrys [2.1] 420, **2008**.
25. Morris GM, Huey R, Lindstrom W, Sanner MF, Belew RK, Goodsell DS, Olson AJ. AutoDock4 and AutoDockTools4: Automated docking with selective receptor flexibility. *J Comput Chem.* **2009**, 30, 2785-91. doi: 10.1002/jcc.21256.